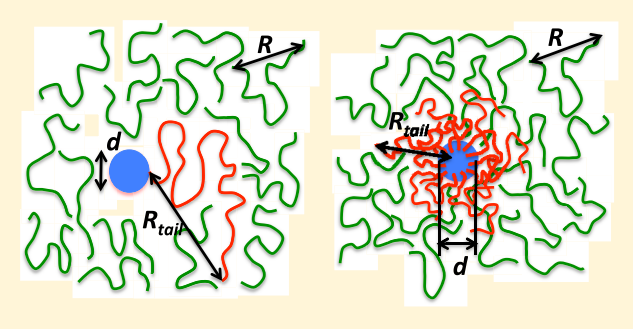
Macromolecules 2019, 52, 1536–1545

# Mobility of Polymer-Tethered Nanoparticles in Unentangled **Polymer Melts**

Ting Ge<sup>†</sup> and Michael Rubinstein\*,†,‡

Department of Mechanical Engineering and Materials Science, Duke University, Durham, North Carolina 27708, United States Departments of Biomedical Engineering, Chemistry, and Physics, Duke University, Durham, North Carolina 27708, United States

ABSTRACT: A scaling theory is developed for the motion of a polymer-tethered nanoparticle (NP) in an unentangled polymer melt. We identify two types of scaling regimes depending on the NP diameter d and the size of a grafted polymer chain (tail)  $R_{\text{tail}}$ . In one type of regime, the tethered NP motion is dominated by the bare NP, as the friction coefficient of the tails is lower than that of the less mobile particle. The time dependence of the mean square displacement (MSD) of the tethered NP  $\langle \Delta r^2(t) \rangle$  in the particle-dominated regime can be approximated by  $\langle \Delta r^2(t) \rangle_{\text{bare}}$  for the bare NP. In the other type of regimes, the tethered NP motion is dominated by the tails when the friction coefficient of the tails



surpasses that of the particle at times longer than the crossover time  $\tau^*$ . In a tail-dominated regime, the MSD  $\langle \Delta r^2(t) \rangle \approx$  $\langle \Delta r^2(t) \rangle_{\text{bare}}$  only for  $t < \tau^*$ .  $\langle \Delta r^2(t) \rangle$  of a single-tail NP for  $t > \tau^*$  is approximated as the MSD  $\langle \Delta r^2(t) \rangle_{\text{tail}}$  of monomers in a free tail, whereas  $\langle \Delta r^2(t) \rangle$  of a multitail NP for  $t > \tau^*$  is approximated as the MSD  $\langle \Delta r^2(t) \rangle_{\text{star}}$  of the branch point of a star polymer. The time dependence of  $\langle \Delta r^2(t) \rangle$  in a tail-dominated regime exhibits two qualitatively different subdiffusive regimes. The first subdiffusive regime for  $t < \tau^*$  arises from the dynamical coupling between the particle and the melt chains. The second subdiffusive regime for  $t > \tau^*$  occurs as the particle participates in the dynamics of the tails. For NPs with loosely grafted chains, there is a Gaussian brush region surrounding the NP, where the chain strands in Gaussian conformations undergo Rouse dynamics with no hydrodynamic coupling. The crossover time  $\tau^*$  for loosely grafted multitail NPs in a tail-dominated regime decreases as the number of tails increases. For NPs with densely grafted chains, the tails are hydrodynamically coupled to each other. The hydrodynamic radii for the diffusion of densely grafted multitail NPs are approximated by the sum of the particle and tail sizes.

# 1. INTRODUCTION

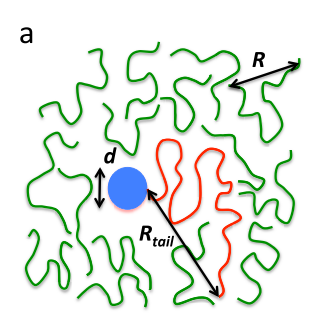
The mobility of particles in a polymeric viscoelastic medium is important to a broad range of applications, including the particle-based microrheology studies of polymer solutions<sup>1,2</sup> and melts,<sup>3–6</sup> the fabrication and processing of nanoparticle polymer composites, <sup>7,8</sup> and the design of drug carriers moving through cells and extracellular matrices. In many cases, the particles are sticky to the surrounding chains due to the attractive interactions between the particles and polymers. For instance, nanoparticles often stick to the polymers in nanocomposites, 10,11 and viruses and pathogens adhere to mucin molecules in the mucus defending human airways and gastrointestinal tract. 12 The attraction between particles and polymers leads to either reversible or permanent adsorption of polymers to the particles. 13,14 The adsorbed chains tend to retard the motion of a sticky particle with respect to that of a nonsticky particle. This has ramifications for the applications relying on the mobility of particles.

In this paper we present a theoretical description of the motion of polymer-tethered nanoparticles (NPs) in an unentangled polymer melt. We consider a NP either with a single polymer chain (tail) or with multiple chains (tails) permanently end-grafted onto it. The grafted chains and the matrix chains in the melt are assumed to be chemically identical. We also assume that there is no adsorption of either grafted chains or matrix chains onto the nanoparticles. Although a single-tail NP rarely occurs in experiments, it serves as a prototype model for the study of how tethered polymers affect NP motion. The research of polymer-tethered NPs provides the first step toward understanding how NP motion is affected by the adsorption layer resulting from the attraction between NPs and surrounding polymers, as the adsorption layer can be mapped to a combination of tails and loops. 15-17

We demonstrate that the motion of a tethered NP in a polymer melt is determined by the competition between the dynamics of the bare NP in the polymer melt and the dynamics of the tethered polymer chains. The theory in this paper is based on the previous scaling theories of the mobility of a nonsticky NP in a polymer melt 18,19 and of polymer dynamics. 20 Through the comparison of the motion of the bare NP and the dynamics of tethered polymer chains, we distinguish particle-dominated and tail-dominated scaling regimes. In a particle-dominated

Received: October 4, 2018 Revised: December 22, 2018 Published: February 6, 2019





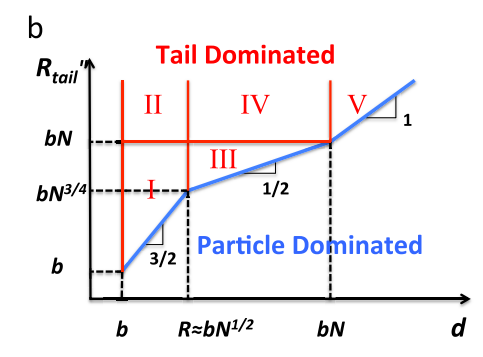


**Figure 1.** (a) Schematic illustration of a NP (blue sphere) with a tethered polymer tail (red line) in a melt of unentangled polymers (green lines). The NP diameter is d. The size of a melt chain is R, while the size of the tail is  $R_{\text{tail}}$ . (b) Scaling regimes in the  $(d,R_{\text{tail}})$  parameter space for the mobility of a single-tail NP in an unentangled polymer melt.

regime, a tethered NP moves as a bare NP, while the effects of the tethered tails on NP motion can be neglected. In a tail-dominated regime, the motion of a tethered NP is not significantly affected by the tails below a crossover time but is dominated by the tails above the crossover time. Section 2 presents the theory for a single-tail NP in an unentangled polymer melt. Section 3 deals with a multitail NP in an unentangled polymer melt. Summary of the results and concluding remarks are in Section 4.

#### 2. NP WITH A SINGLE TAIL

We first consider a NP with a grafted polymer chain (a tail) diffusing in an unentangled polymer melt, as illustrated in Figure 1a. The diameter of the NP is d, and its mass is m. Kuhn lengths of the grafted chain and of the melt chains are both b. The number of Kuhn segments in the tail is  $N_{\rm tail}$ , while the number of Kuhn segments per melt chain is N. The root-mean-square end-to-end size of a melt chain is  $R \approx bN^{1/2}$ . The root-mean-square end-to-end size of the tail  $R_{\rm tail} \approx bN_{\rm tail}^{1/2}$  for  $N_{\rm tail} < N^2$ , obeying the ideal random-walk statistics. A longer tail with  $N_{\rm tail} > N^2$  is expected to swell in the melt, and  $R_{\rm tail} \approx bN(N_{\rm tail}/N^2)^{3/5}$ , corresponding to a self-avoiding random-walk conformation of chain sections each containing  $N^2$  Kuhn segments. Throughout the paper, we ignore any order-unity prefactors while focusing on the scaling relations and use the sign  $\approx$  to indicate equality on the scaling level.

The diffusion coefficient D quantifies the mobility of a single-tail NP. According to the Stokes—Einstein relation, D is related to the friction coefficient  $\zeta$ 

$$D \approx \frac{k_{\rm B}T}{\zeta} \tag{1}$$

in which  $k_{\rm B}$  is the Boltzmann constant, and T is the absolute temperature. We determine the friction coefficient  $\zeta$  on the basis of the previous scaling theories for the friction coefficients  $\zeta_{\rm bare}$  of a bare NP without the tail 18,19 and  $\zeta_{\rm tail}$  of a free tail without the particle. For the diffusion of a bare NP in an unentangled polymer melt

$$\zeta_{\text{bare}} \approx \begin{cases} \eta_0 \left(\frac{d}{b}\right)^2 d \approx \zeta_0 \left(\frac{d}{b}\right)^3 & \text{for } b < d < R \\ \eta_0 \left(\frac{R}{b}\right)^2 d \approx \zeta_0 \left(\frac{R}{b}\right)^2 \left(\frac{d}{b}\right) & \text{for } d > R \end{cases}$$
(2)

where  $\eta_0$  is the monomeric viscosity, and  $\zeta_0 \approx \eta_0 b$  is the monomeric friction coefficient. A small bare NP with b < d < R

does not experience the viscosity  $\approx \eta_0 N \approx \eta_0 (R/b)^2$  of the polymer melt, but only an effective viscosity  $\approx \eta_0 (d/b)^2$  corresponding to polymer chain sections whose sizes  $\approx d$ . In contrast, a large bare NP with d > R experiences the full polymer melt viscosity  $\approx \eta_0 N$  independent of d. For the diffusion of a free tail in an unentangled polymer melt

$$\zeta_{\text{tail}} \approx \begin{cases}
\zeta_0 N_{\text{tail}} \approx \zeta_0 \left(\frac{R_{\text{tail}}}{b}\right)^2 & \text{for } b < R_{\text{tail}} < Nb \\
\zeta_0 N^2 \left(\frac{R_{\text{tail}}}{Nb}\right) & \text{for } R_{\text{tail}} > Nb
\end{cases}$$
(3)

 $\zeta_{\rm tail}$  is proportional to the number of monomers  $N_{\rm tail}$  in the tail if the melt chains screen the hydrodynamic coupling between sections of the tail with  $b < R_{\rm tail} < Nb$ .  $\zeta_{\rm tail}$  for a longer tail with  $R_{\rm tail} > Nb$  scales with the size of the tail  $R_{\rm tail}$  due to the unscreened hydrodynamic coupling between sections of the tail. <sup>20</sup> For  $R_{\rm tail} > Nb$ , the friction of the tail  $\zeta_{\rm tail} \approx \zeta_0 N^2 (R_{\rm tail}/Nb) \approx \zeta_0 N_{\rm tail}^{3/5} N^{4/5}$  resulting from the hydrodynamic coupling is smaller than  $\zeta_{\rm tail} \approx \zeta_0 N_{\rm tail}$  without hydrodynamic coupling, and thus is a more favorable way of energy dissipation.

Since the bare NP is dynamically coupled to a wake of size  $\approx d$  in the melt surrounding the particle, adding a small tail with  $R_{\rm tail} < d$  to the wake does not significantly change the motion of the particle with respect to that of the bare NP. As a result, the friction coefficient  $\zeta$  of the single-tail NP with  $R_{\rm tail} < d$  is approximated as  $\zeta_{\rm bare}$  of a bare NP, and the mobility of the single-tail NP is dominated by the particle with  $D \approx k_{\rm B}T/\zeta_{\rm bare}$ . If  $R_{\rm tail} > d$ , a significant portion of the tail is beyond the wake surrounding the particle. The friction coefficient of the single-tail NP is approximated as

$$\zeta \approx \zeta_{\text{bare}} + \zeta_{\text{tail}}$$
 (4)

where  $\zeta_{\text{bare}}$  and  $\zeta_{\text{tail}}$  are given in eq 2 and eq 3, respectively. The diffusion coefficient for a single-tail NP is

$$D \approx \frac{k_{\rm B}T}{\zeta_{\rm bare} + \zeta_{\rm tail}} \tag{5}$$

If  $\zeta_{\text{tail}} \ll \zeta_{\text{bare}}$ , the diffusion of the particle is not significantly affected by the tail, as the tail with a smaller friction coefficient is more mobile than the particle. Therefore, D is approximated as the diffusion coefficient for the bare NP

$$D pprox rac{k_{
m B}T}{\zeta_{
m bare}} pprox D_{
m bare} \quad {
m for} \quad \zeta_{
m tail} \ll \zeta_{
m bare}$$
 (6)

If  $\zeta_{\text{tail}}$  is comparable to  $\zeta_{\text{bare}}$ , the effects of the tail on the diffusion of the particle cannot be ignored. The expression in eq 5 can be used to approximate D. If  $\zeta_{\text{tail}} \gg \zeta_{\text{bare}}$ , the diffusion of the single-tail NP is controlled by the tail that has a higher friction coefficient. As a result, D is approximated as the diffusion coefficient for the free tail

$$D pprox rac{k_{
m B}T}{\zeta_{
m tail}} pprox D_{
m tail} \quad {
m for} \quad \zeta_{
m tail} \gg \zeta_{
m bare}$$
 (7)

For  $R_{\rm tail} > d$ , the two friction coefficients  $\zeta_{\rm tail}$  and  $\zeta_{\rm bare}$  are compared to determine if the diffusion of a single-tail NP is controlled by the particle with  $D_{\rm tail} > D_{\rm bare}$  or by the tail with  $D_{\rm tail} < D_{\rm bare}$ . Whether the combined friction coefficient  $\zeta$  (eq 4) for a single-tail NP is dominated by  $\zeta_{\rm bare}$  or  $\zeta_{\rm tail}$  depends on d and  $R_{\rm tail}$ . In the parameter space  $(d,R_{\rm tail})$ , the boundary line with  $\zeta_{\rm tail} \approx \zeta_{\rm bare}$  separates the regions where the diffusion of the single-tail NP is controlled by the particle and the tail, respectively. The boundary line is

$$R_{\text{tail}} \approx \begin{cases} b \left(\frac{d}{b}\right)^{3/2} \approx d \left(\frac{d}{b}\right)^{1/2} & \text{for } b < d < R \approx bN^{1/2} \\ bN^{1/2} \left(\frac{d}{b}\right)^{1/2} & \text{for } R < d < bN \\ d & \text{for } d > bN \end{cases}$$
(8)

Note that the particle and the sections of the tail are hydrodynamically coupled for  $R_{\rm tail} > d > bN$ . The friction coefficient of the single-tail NP  $\zeta$  is approximated as  $\zeta_{\rm tail}$ , as the size or the hydrodynamic radius of the tail is larger than that of the particle. The mobility of the single-tail NP is dominated by the tail with  $D \approx k_{\rm B}T/\zeta_{\rm tail}$ .

On time scales shorter than the onset of terminal diffusion, the motion of a single-tail NP is quantified by the time dependence of its mean square displacement (MSD)  $\langle \Delta r^2(t) \rangle$ . For  $R_{\rm tail} < d$ , the motion of the particle is not significantly affected by the attached tail, and therefore  $\langle \Delta r^2(t) \rangle$  is approximated as the MSD of a bare NP  $\langle \Delta r^2(t) \rangle_{\rm bare}$ . For  $R_{\rm tail} > d$ , the MSD

$$\langle \Delta r^2(t) \rangle \approx \frac{k_{\rm B}T}{\zeta(t)} t \approx \frac{k_{\rm B}T}{\zeta_{\rm bare}(t) + \zeta_{\rm tail}(t)} t$$
 (9)

where the time-dependent effective friction coefficient  $\zeta(t)$  includes  $\zeta_{\rm bare}(t)$  for the bare NP and  $\zeta_{\rm tail}(t)$  for a chain section of g(t) monomers that move coherently with each other on time scale t. Similar to eq 6 and eq 7 for terminal diffusion

$$\begin{split} \langle \Delta r^2(t) \rangle &\approx \frac{k_{\rm B} T}{\max\{\zeta_{\rm bare}(t),\,\zeta_{\rm tail}(t)\}} \\ &\approx \begin{cases} \frac{k_{\rm B} T}{\zeta_{\rm bare}(t)} t \approx \langle \Delta r^2(t) \rangle_{\rm bare} & \text{for } \zeta_{\rm tail}(t) \ll \zeta_{\rm bare}(t) \\ \frac{k_{\rm B} T}{\zeta_{\rm tail}(t)} t \approx \langle \Delta r^2(t) \rangle_{\rm tail} & \text{for } \zeta_{\rm tail}(t) \gg \zeta_{\rm bare}(t) \end{cases} \end{split}$$

In Appendix A, we present the scaling results for  $\langle \Delta r^2(t) \rangle_{\rm bare}$  (eqs. A.1, A.2, and A.6) and  $\langle \Delta r^2(t) \rangle_{\rm tail}$  (eqs. A.7—A.10).  $\langle \Delta r^2(t) \rangle_{\rm bare}$  and  $\langle \Delta r^2(t) \rangle_{\rm tail}$  are compared to identify different scaling regimes for the motion of a single-tail NP with  $R_{\rm tail} > d$  in an unentangled polymer melt.

As shown in Figure 1b, there is a particle-dominated regime below the blue solid line, where both the terminal diffusion of the single-tail NP and the motion prior to the diffusion are controlled by the particle with  $\langle \Delta r^2(t) \rangle \approx \langle \Delta r^2(t) \rangle_{\rm bare}.$  In the particle-dominated regime, the tail does not significantly affect the particle dynamics at all time scales. There are five different tail-dominated regimes depending on the NP size d and the tail size  $R_{\rm tail}.$  In each regime, there is a crossover from the particle-dominated motion at shorter time scales to the tail-dominated motion as t increases. At the crossover time  $\tau^*, \langle \Delta r^2(\tau^*) \rangle_{\rm bare} \approx \langle \Delta r^2(\tau^*) \rangle_{\rm tail}.$  For regimes I–IV, the friction coefficients  $\zeta_{\rm bare}(\tau^*)$  for the bare NP and  $\zeta_{\rm tail}(\tau^*)$  for the chain section of  $g(\tau^*)$  coherently moving monomers are comparable to each other. The results of  $\tau^*$  for the five tail-dominated regimes are listed in Table 1 and plotted as a function of d in Figure 2. At time scales

Table 1. Crossover Time  $au^*$  for a Single-Tail NP in an Unentangled Polymer Melt

regimes I and II	regimes III and IV	regime V
$ au_{I,II}^* pprox  au_0 (d/b)^6$	$\tau_{III,IV}^* \approx \tau_0 (d/b)^2 (R/b)^4$	$\tau_V^* \approx \tau_0 N(d/b)^3$

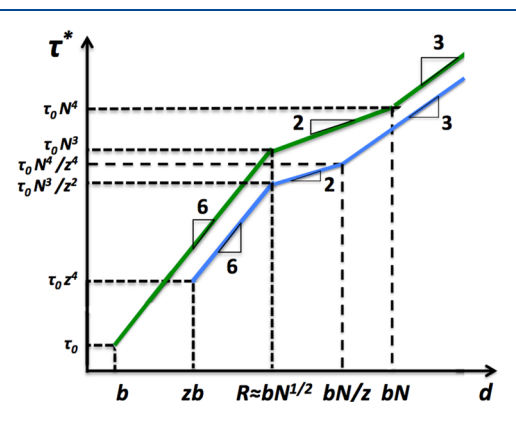


**Figure 2.** Dependence of the crossover time  $\tau^*$  (see Table 1 and Table 2) on the particle diameter d for a single-tail NP (green upper line) and a NP loosely grafted with  $1 < z < N^{1/2}$  tails (blue lower line) in an unentangled polymer melt.

shorter than  $\tau^*$ , the single-tail NP motion is controlled by the particle. The single-tail NP behaves as a bare NP with  $\langle \Delta r^2(t) \rangle \approx$  $\langle \Delta r^2(t) \rangle_{\text{bare}} < \langle \Delta r^2(t) \rangle_{\text{tail}}$ . The time dependence of  $\langle \Delta r^2(t) \rangle_{\text{bare}}$  is  $\langle \Delta r^2(t) \rangle_{\text{bare}} \sim t^2$  for the ballistic particle motion at time scales shorter than the ballistic time  $\tau_{\rm bal}$   $\langle \Delta r^2(t) \rangle_{\rm bare} \sim t^{1/2}$  for the subdiffusive motion resulting from the coupling to the Rouse dynamics of the melt chains at time scales between  $au_{\rm bal}$  and the diffusion time  $\tau_{\rm d}$ , and  $\langle \Delta r^2(t) \rangle_{\rm bare} \sim t$  for the diffusive particle motion at time scales between  $\tau_d$  and  $\tau^*$ . The three distinctive time dependences of  $\langle \Delta r^2(t) \rangle$  for  $t < \tau^*$  are sketched in Figure 3 for the five regimes. At time scales longer than  $au^*$ , the dynamics of the tail dominates the single-tail NP motion. The particle follows the tail dynamics, and  $\langle \Delta r^2(t) \rangle \approx \langle \Delta r^2(t) \rangle_{\text{tail}} < 1$  $\langle \Delta r^2(t) \rangle_{\rm bare}$ . For regimes I and III with  $b < R_{\rm tail} < bN$ , the particle participates in the Rouse dynamics of the tail with  $\langle \Delta r^2(t) \rangle_{\rm tail}^{\prime} \sim t^{1/2}$  at time scales between  $\tau^*$  and the Rouse time  $au_{
m R,tail}$  and then diffuses with  $\langle \Delta r^2(t) \rangle_{
m tail} \sim t$  for  $t > au_{
m R,tail}$ . The subdiffusive motion with  $\langle \Delta r^2(t) \rangle \sim t^{1/2}$  occurs in two time ranges, as shown in Figure 3a. The first one for  $\tau_{\text{bal}}^{I}(\tau_{\text{bal}}^{III}) < t < 1$  $au_{
m d}^{I}( au_{
m d}^{III})$  results from the coupling between the NP motion and the Rouse dynamics of surrounding polymers in the melt. The second one in  $\tau_I^*(\tau_{III}^*) < t < \tau_{R,tail}$  arises from the Rouse relaxation modes of the tail. For regimes II, IV, and V with  $R_{tail} > bN$ , the motion of the tail changes from Rouse dynamics with  $\langle \Delta r^2(t) \rangle_{\text{tail}}$  $\sim t^{1/2}$  to Zimm dynamics with  $\langle \Delta r^2(t) \rangle_{\text{tail}} \sim t^{2/3}$  at the crossover

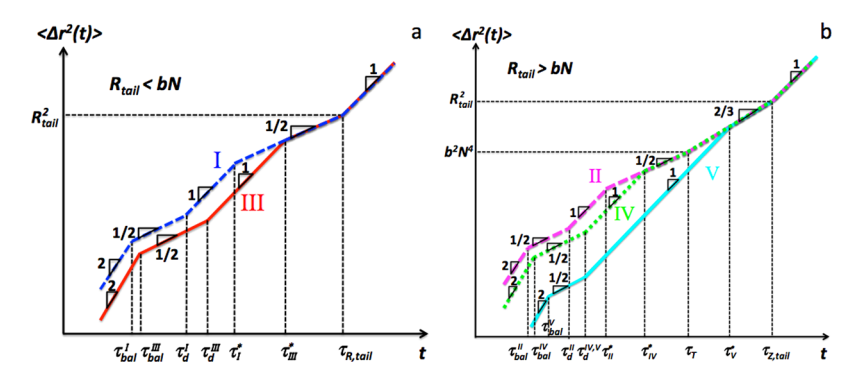
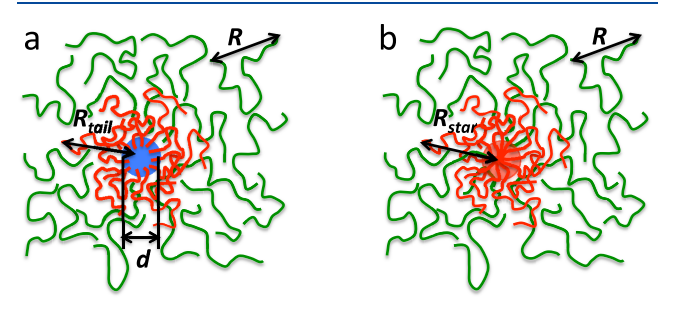


Figure 3. Time dependence of the MSD  $\langle \Delta r^2(t) \rangle$  of a single-tail NP in an unentangled polymer melt for (a) regimes I and III and (b) regimes II, IV, and V in Figure 1b.

time  $\tau_{\mathrm{T}}$ . Whether a particle participates in the Rouse dynamics of such a long tail depends on whether  $\tau^*$  is smaller than  $\tau_{\mathrm{T}}$ . As shown in Figure 3b, a particle in regime II or IV participates in the Rouse dynamics for  $\tau_{\mathrm{II}}^*(\tau_{\mathrm{IV}}^*) < t < \tau_{\mathrm{T}}$  and then the Zimm dynamics for  $\tau_{\mathrm{T}} < t < \tau_{\mathrm{Z,tail}}$ , whereas a particle in regime V only participates in the Zimm dynamics for  $\tau_{\mathrm{V}}^* < t < \tau_{\mathrm{Z,tail}}$ . The singletail NP finally diffuses with  $\langle \Delta r^2(t) \rangle \approx \langle \Delta r^2(t) \rangle_{\mathrm{tail}} \sim t$  for  $t > \tau_{\mathrm{Z,tail}}$ . The details of the calculation of  $\langle \Delta r^2(t) \rangle$  and the features of  $\langle \Delta r^2(t) \rangle$  for different regimes are presented in Appendix A.

#### 3. NP WITH MULTIPLE TAILS

A NP with multiple grafted chains is illustrated in Figure 4a. The conformations of the tails grafted to the NP are similar to the



**Figure 4.** (a) Schematic illustration of a NP (blue sphere) with z > 1 grafted tails (red lines) in a melt of unentangled polymers (green lines) with N monomers per chain. The NP diameter is d. The size of a melt chain is  $R \approx b N^{1/2}$ , while the size of the tail is  $R_{\text{tail}}$ . The multitail NP in (a) is mapped to a star polymer in the same melt, as illustrated in (b). The number of arms in the star is z. The size of the star is  $R_{\text{star}} \approx R_{\text{tail}}$ . The red sphere in (b) indicates the inner region of the star with diameter  $\approx d$ .

conformations of the arms in the outer part (the part excluding the inner region of size  $\approx d$ ) of a star polymer in the same melt, as shown in Figure 4b. Previously, scaling theories  $^{21-24}$  have been developed to describe the static properties of an isolated star polymer with z arms and  $N_{\rm a}$  monomers per arm dissolved in a melt of chemically identical linear chains with N monomers per chain. Below we first briefly review the existing theories for the conformations of star polymers and then develop a new scaling theory for the mobility of a multitail NP on the basis of mapping a multitail NP to a star polymer.

According to the scaling theories,  $^{21-24}$  the radius and the structure of a star polymer in a melt depend on the number of arms z and the number of monomers  $N_{\rm a}$  per arm, as shown in Figure 5. For a loosely branched star with  $1 < z < N^{1/2}$  arms, the radius of the star

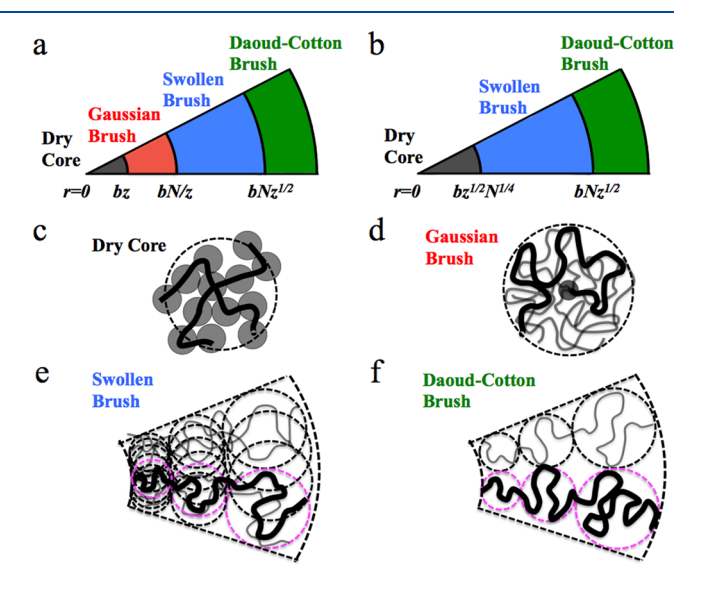


Figure 5. Locations of different regions in (a) a loosely branched star polymer with  $1 < z < N^{1/2}$  arms and (b) a densely branched star polymer with  $z > N^{1/2}$  arms in a linear polymer melt with N monomers per chain. In both scenarios, only a star consisting of sufficiently long arms with the number of monomers per arm  $N_a > N^2 z^{1/2}$  contains all the sketched regions. The structure of a dry core is illustrated in (c), where filled circles and black thick lines indicate the monomers and backbones, respectively. The conformations of chain sections in the Gaussian brush, swollen brush, and Daoud-Cotton brush are illustrated in (df), respectively. The filled circle in (d) indicates the dry core surrounded by the Gaussian brush. For each type of brush, the strand belonging to one arm is highlighted by the black thick line. Dashed circles in (e, f) indicate the correlation blobs with sizes growing along the radial axis. Magenta dashed circles in (e, f) indicate the correlation blobs of the arm highlighted by the black solid line. Multiple chain strands exist in a correlation blob of a swollen brush, and the correlation blobs of different strands overlap, as illustrated in (e). By contrast, only one chain strand occupies a correlation blob of a Daoud-Cotton brush, as illustrated in (f). In a correlation blob, the excluded volume interaction of a chain strand with other strands at the same length scale is on the order of thermal energy  $k_{\rm B}T$ .

$$R_{\text{star}} \approx \begin{cases} b(zN_{\text{a}})^{1/3} & \text{for } N_{\text{a}} < z^{2} \\ bN_{\text{a}}^{1/2} & \text{for } z^{2} < N_{\text{a}} < (N/z)^{2} \\ bN_{\text{a}}^{3/5} (z/N)^{1/5} & \text{for } N_{\text{a}} > (N/z)^{2} \end{cases}$$
(11)

If the arms are short with  $N_{\rm a} < z^2$ , the star is dry with almost no mixing with the melt chains; that is, the volume fraction of monomers belonging to the star  $\approx 1$ . The arms of the dry star and

the arm strands in the dry core of a larger star are stretched with respect to their ideal Gaussian sizes. The stretching is due to the steric hindrance between all the arms originating from the same branch point, as illustrated in Figure 5c. The radius of the dry star  $R_{\text{star}} \sim (zN_a)^{1/3}$ . If  $z^2 < N_a < (N/z)^2$ , the star consists of a brush corona surrounding a dry core of size  $\approx bz$ , which contains  $z^2$  monomers per arm. Chain segments in the brush corona adopt ideal random-walk conformations, as the excluded volume interactions between the arms are almost screened by the melt chains. Such a Gaussian brush with  $R_{\rm star} \sim N_{\rm a}^{1/2}$  is illustrated in Figure 5d. If the arms are long with  $N_{\rm a} > (N/z)^2$ , the brush corona covering the dry core contains an inner Gaussian brush and an outer brush, where chain segments adopt swollen conformations. The size of the Gaussian brush region  $\approx bN/z$ , which corresponds to  $(N/z)^2$  monomers per arm. The overall star radius  $R_{\text{star}} \sim N_a^{3/5} (z/N)^{1/5}$ . For  $(N/z)^2 < N_a < N^2 z^{1/2}$ , there are multiple chain sections of Gaussian conformations in a correlation blob of a swollen brush, as shown in Figure 5e. Multiple chain sections are required to make the overall excluded volume interaction of a chain strand in a correlation blob  $\approx k_{\rm B}T$ , because the excluded volume interactions are partially screened by the melt chains. For  $N_a > N^2 z^{1/2}$ , there is also a swollen brush with multiple chain sections per correlation blob at intermediate distances  $bN/z < r < bNz^{1/2}$  from the branch point. However, each correlation blob at  $r > bNz^{1/2}$ contains only one chain section, as shown in Figure 5f. The chain section in a blob adopts a swollen conformation, as the blob size  $\xi(r) \approx r/z^{1/2}$  is larger than the thermal blob size  $\approx bN$  for r > 1 $bNz^{1/2}$ . The brush structure for  $r > bNz^{1/2}$  can be described using the model proposed by Daoud and Cotton.<sup>21</sup> The Daoud-Cotton brush corona only exists in a star polymer with  $N_a$  >  $N^2z^{1/2}$ . The locations of different regions along the radial axis of a loosely branched star with sufficiently long arms are shown in Figure 5a. For a densely branched star with  $z > N^{1/2}$ , the radius of the star

$$R_{\text{star}} \approx \begin{cases} b(zN_a)^{1/3} & \text{for } N_a < z^{1/2}N^{3/4} \\ bN_a^{3/5}(z/N)^{1/5} & \text{for } N_a > z^{1/2}N^{3/4} \end{cases}$$
 (12)

If the arms are short with  $N_{\rm a} < z^{1/2} N^{3/4}$ , the star is dry with  $R_{\rm star} \sim (zN_{\rm a})^{1/3}$ . If the arms are long with  $N_{\rm a} > z^{1/2} N^{3/4}$ , the star consists of a dry core surrounded by a brush corona. The size of the core  $\approx bz^{1/2} N^{1/4}$ , corresponding to  $z^{1/2} N^{3/4}$  monomers per arm, while the overall star radius  $R_{\rm star} \sim N_{\rm a}^{3/5} (z/N)^{1/5}$ . As in a loosely branched star, the Daoud—Cotton brush exists in a densely branched star only for  $N_{\rm a} > N^2 z^{1/2}$ . The locations of different regions along the radial axis of a densely branched star with  $N_{\rm a} > N^2 z^{1/2}$  are shown in Figure 5b. Unlike the brush corona of a loosely branched star, the brush corona of a densely branched star does not contain a Gaussian brush region. There is no intermediate range of  $N_{\rm a}$  for which the star contains a dry core and a Gaussian brush corona, because the screening by the melt chains is not strong enough to reduce the overall exclude volume interaction between all densely branched arms below  $k_{\rm B}T$  per arm.

We develop a scaling theory for the motion of a multitail NP in an unentangled polymer melt by considering a star polymer with z arms and arm length  $N_{\rm a}\approx N_{\rm tail}$  in the same melt (see Figure 4). Similar to the motion of a single-tail NP, the motion of a multitail NP is significantly affected by the tails only if  $R_{\rm tail}>d$ . Therefore, below we only describe the motion of a multitail NP

with  $R_{\text{tail}} > d$ . The motion of a multitail NP with  $R_{\text{tail}} < d$  can be approximated as that of a bare NP.

**3.1. Loosely Grafted Tails with 1** < z <  $N^{1/2}$ . If the grafted tails are short with d <  $R_{tail}$  < bz, a multitail NP corresponds to a dry star polymer. The size of this multitail NP  $\approx R_{tail} \approx bN_{tail}^{1/3}z^{1/3}$  (see eq 11 for a dry star with  $N_a$  <  $z^2$ ). As demonstrated in Appendix B, although the position of the particle fluctuates under the confinement of the grafted dry tails, the motion of the multitail NP can be approximated as that of a larger particle with diameter  $\approx R_{tail}$  in the matrix of melt chains. This tail-dominated regime with d <  $R_{tail}$  < bz is indicated as regime VI of the  $(d,R_{tail})$  parameter space in Figure 6.

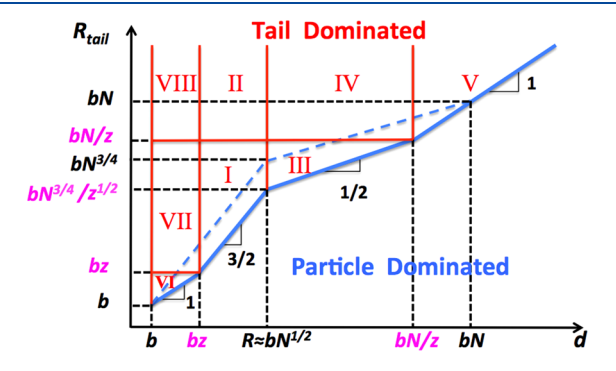


**Figure 6.** Scaling regimes in the  $(d_nR_{\rm tail})$  parameter space for the mobility of a NP with  $1 < z < N^{1/2}$  tails in an unentangled polymer melt. Blue solid and dashed lines indicate the boundaries between tail-dominated regimes and the particle-dominated regimes for a multitail NP and a single-tail NP (also Figure 1b), respectively. Red solid lines indicate the boundaries between different tail-dominated regimes for a multitail NP.

A multitail NP with intermediate tail size in the range  $\max\{d,bz\}$  <  $R_{\text{tail}}$  < bN/z corresponds to a star polymer consisting of a dry core and a Gaussian brush corona. The size of the multitail NP is  $\approx R_{\text{tail}} \approx b N_{\text{tail}}^{1/2}$  (see eq 11 for a star with  $z^2$  <  $N_a < (N/z)^2$ ). If d < bz, the multitail NP motion is controlled by the tails, as the particle and the dry portions of the tails move together as a larger particle with diameter  $\approx bz$ . This corresponds to regime VII in Figure 6. The MSD of the multitail NP in this regime is  $\langle \Delta r^2(t) \rangle \approx (b^2/z)(t/\tau_0)^{1/2}$  for  $t < \tau_0 z^4$  (substitute  $R_{\text{tail}}$ by bz in eq B.1). Note that  $\tau_0 z^4$  is the Rouse time of a segment containing  $z^2$  monomers in the dry core of a star polymer. At times longer than  $\tau_0 z^4$ ,  $\langle \Delta r^2(t) \rangle$  is approximately the same as  $\langle \Delta r^2(t) \rangle_{\text{star}}$  of the branch point of a Gaussian star. If d > bz, the tails do not contain any dry portions. Whether the multitail NP motion is controlled by the particle or the tails in the Gaussian brush depends on the competition of the friction coefficients of the bare particle and the tails. The friction coefficient of the bare particle  $\hat{\zeta}_{\text{bare}}$  is given in eq 2. The friction coefficient of the tails  $\approx z\zeta_{\text{tail}}$ , where  $\zeta_{\text{tail}} \approx \zeta_0 N_{\text{tail}} \approx \zeta_0 (R_{\text{tail}}/b)^2$  is the friction coefficient of a single tail undergoing Rouse dynamics. The friction coefficients for individual tails are additive due to the absence of hydrodynamic coupling between the tails. The overall friction coefficient of the multitail NP is approximated as

$$\zeta \approx \zeta_{\text{bare}} + z\zeta_{\text{tail}}$$
 for  $1 < z < N^{1/2}$  and  $bz < d < R_{\text{tail}} < bN/z$  (13)

 $\zeta$  is dominated by the larger of the two contributions  $\zeta_{\rm bare}$  and  $z\zeta_{\rm tail}$ . In the parameter space  $(d,R_{\rm tail})$ , the boundary line separating the regions where the diffusion of a multitail NP is

dominated, respectively, by the particle and the Gaussian brush is

$$R_{\text{tail}} \approx \begin{cases} \frac{b}{z^{1/2}} \left(\frac{d}{b}\right)^{3/2} & \text{for } zb < d < R \approx bN^{1/2} \\ \frac{bN^{1/2}}{z^{1/2}} \left(\frac{d}{b}\right)^{1/2} & \text{for } R < d < bN/z \end{cases}$$
(14)

as indicated by the blue solid line in Figure 6. Two regimes, which are indicated as regimes I and III in Figure 6, exist in the tail-dominated region with  $bz < d < R_{\rm tail} < bN/z$ . Regimes I and III for multitail NP motion are similar to their counterparts for single-tail NP motion (see Figure 1b). The time dependence of  $\langle \Delta r^2(t) \rangle$  is similar to that in the corresponding regime for single-tail NP motion (Figure 3a). However, the crossover time  $\tau^*$  for multitail NP motion is reduced with respect to the corresponding  $\tau^*$  for single-tail NP motion, as shown in Table 2 and Figure 2. The earlier crossover to the tail-dominated

Table 2. Crossover Time  $\tau^*$  for a NP Loosely Grafted with  $1 < z < N^{1/2}$  Tails in an Unentangled Polymer Melt

regimes I and II	regimes III and IV	regime V
$ au_{I,II}^* pprox  au_0 (d/b)^6/z^2$	$ au_{III,IV}^* pprox  au_0 (d/b)^2 (R/b)^4/z^2$	$\tau_V^* \approx \tau_0 N(d/b)^3/z$

motion reflects the enhanced friction coefficient of multiple tails compared to that of a single tail. For  $t > \tau^*$ , the multitail NP MSD  $\langle \Delta r^2(t) \rangle$  is approximately equal to the MSD  $\langle \Delta r^2(t) \rangle_{\text{star}}$  of the branch point of a Gaussian star polymer.

For sufficiently long tails with  $R_{\text{tail}} > \max\{d,bN/z\}$ , a multitail NP corresponds to a star polymer consisting of a dry core, an intermediate Gaussian brush, and an outer brush corona ("hairy" NP). The size of the multitail NP is  $\approx R_{tail} \approx$  $bN_{\text{tail}}^{3/5}(z/N)^{1/5}$  (see eq 11 for a star with  $N_a > (N/z)^2$ ). In a star polymer with arms forming either a swollen brush corona (Figure 5e) or a Daoud-Cotton brush corona (Figure 5f) covering a swollen brush, hydrodynamical coupling between the arms affects the branch point motion for t above the Rouse time  $\approx \tau_0 (N/z)^4$  of a strand in the Gaussian brush. In particular, the arms are hydrodynamically coupled for the terminal diffusion of the star. Likewise, a multitail NP with  $R_{\text{tail}} > \max\{d,bN/z\}$ diffuses in the melt with the NP and the tails hydrodynamically coupled. The hydrodynamic radius of the multitail NP can be approximated by the sum of  $R_{\text{tail}}$  and d, which is dominated by  $R_{\text{tail}} > d$ . The multitail NP experiences the melt viscosity  $\eta_0 N$ , as its size  $\approx R_{\text{tail}} > bN/z$  is larger than the melt chain size  $R \approx bN^{1/2}$ . The diffusion coefficient of the multitail NP is  $D \approx k_B T/$  $(\eta_0 NR_{tail})$ . There are four regimes in the tail-dominated region with  $R_{\text{tail}} > bN/z$ , which are indicated as regimes II, IV, V, and VIII in Figure 6. Regimes II, IV, and V for multitail NP motion are similar to their counterparts for single-tail NP motion (see Figure 1b for the regimes and Figure 3b for the sketch of  $\langle \Delta r^2(t) \rangle$ ). However, the crossover time  $\tau^*$  is reduced as shown in Table 2 and Figure 2. The time for the crossover from Rouse dynamics to Zimm dynamics of the hydrodynamically coupled tails is also reduced from  $\tau_{\rm T} \approx \tau_0 N^4$  for a single tail to  $\tau_{\rm T} \approx \tau_0 (N/z)^4$ , which is the Rouse time of a chain segment containing  $(N/z)^2$  monomers in the Gaussian brush (Figure 5d). In regime VIII, the particle with d < bz and the dry portions of the tails move as a larger particle with diameter  $\approx bz$ , and thus the multitail NP motion is controlled by the tails. As in regime VII, the multitail NP MSD  $\langle \Delta r^2(t) \rangle \approx (b^2/z)(t/\tau_0)^{1/2}$  for  $t < \infty$ 

 $\tau_0 z^4$ . At time scales above  $\tau_0 z^4$ ,  $\langle \Delta r^2(t) \rangle$  is approximately the same as  $\langle \Delta r^2(t) \rangle_{\rm star}$  of the branch point of the corresponding star polymer.

**3.2. Densely Grafted Tails with z** >  $N^{1/2}$ . If the grafted tails are short with  $d < R_{tail} < bz^{1/2}N^{1/4}$ , a densely grafted multitail NP corresponds to a dry star in the same melt (see eq 12 for  $N_a < z^{1/2}N^{3/4}$ ). The multitail NP motion is similar to that in regime VI for loosely grafted multitail NPs (see Figure 6). It is controlled by the tails, as the particle and the dry tails move together as a larger particle with diameter  $\approx R_{tail}$ . More detailed analysis is presented in Appendix B. The MSD of a multitail NP before the terminal diffusion in this regime is given in eq 2.

A densely grafted multitail NP with long tails of size  $R_{\rm tail} > \max\{d,bz^{1/2}N^{1/4}\}$  corresponds to a star consisting of a dry core and a brush corona (either a swollen brush or Daoud–Cotton brush covering a swollen brush). The particle and the tails are hydrodynamically coupled for the diffusion of the multitail NP. The hydrodynamic radius can be approximated by the sum of the tail size  $R_{\rm tail}$  and the particle size d, and it is dominated by  $R_{\rm tail} > d$ . The viscosity experienced by the multitail NP is the melt viscosity  $\eta N$ , as  $R_{\rm tail} > bz^{1/2}N^{3/4}$  is larger than the melt chain size  $R \approx bN^{1/2}$ . The diffusion coefficient is  $D \approx k_{\rm B}T/(\eta NR_{\rm tail})$ .

Various aspects of the dynamics of grafted nanoparticles in polymer matrices have been studied experimentally, such as the effects of temperature, <sup>25,26</sup> morphology of particles in aggregated state, <sup>27</sup> and grafted polymer chains. <sup>28,29</sup> We compare the theory developed in this paper with one experimental study that focused on the effects of grafted polymers.<sup>29</sup> In this study, the center-of-mass diffusion of Fe<sub>3</sub>O<sub>4</sub> NPs densely grafted with poly(methyl methacrylate) (PMMA) chains in an unentangled PMMA melt was measured using Rutherford backscattering spectrometry (RBS).<sup>29</sup> In one set of experiments, Fe<sub>3</sub>O<sub>4</sub> NPs with diameter d = 4.3 nm were grafted with PMMA chains and dispersed in a melt of PMMA chains with molecular weight  $M_w =$ 14 kg/mol, which corresponds to N = 26 Kuhn monomers of size b = 1.53 nm.<sup>30</sup> There were three samples with grafting density  $\sigma = 0.55$ , 0.33, and 0.17 chains/nm<sup>2</sup>. The number of grafted tails per NP is  $z = \pi d^2 \sigma = 32$ , 19, and 10, and the corresponding number of Kuhn monomers per tail is  $N_{\text{tail}} = 30$ , 39, and 39. We refine the criterion for a loosely grafted NP in a melt matrix and show that the NPs in all three samples are indeed not loosely grafted. The criterion  $z < N^{1/2}$  for a loosely grafted NP corresponds to the existence of a Gaussian star with  $R_{\rm star} \approx b N_{\rm a}^{1/2}$  for  $z^2 < N_{\rm a} < (N/z)^2$ , as shown in eq 11. A strand with less than  $z^2$  Kuhn monomers from the branch point is located in the dry core, while a strand with more than  $(N/z)^2$ Kuhn monomers from the branch point goes beyond the Gaussian region and becomes swollen. The expression for the size of a dry star  $R_{\text{star}} \approx b(zN_a)^{1/3}$  for  $N_a < z^2$  (eq 11) is refined by considering that the volume of a Kuhn monomer is not  $b^3$  but more precisely  $ba^2$ , where a is the thickness of a Kuhn monomer. The refined expression is  $R_{\rm star} \approx a^{2/3} b^{1/3} (z N_{\rm a})^{1/3}$  for  $N_{\rm a} <$  $z^{2}(a/b)^{4}$ . The refined criterion for the existence of a Gaussian star is  $z^2(a/b)^4 < N_a < (N/z)^2$ , which requires  $z < (b/a)N^{1/2}$ . Accordingly, the refined criterion for a loosely grafted NP is z < $(b/a)N^{1/2}$ . For the three samples in the experiments, the volume of a monomer is v = 0.149 nm<sup>3</sup>, the molecular weight of a monomer is  $M_0 = 0.1$  kg/mol, the molecular weight of a Kuhn monomer is  $M_k = 0.54$  kg/mol, and hence the thickness of a Kuhn monomer is  $a = (M_k \nu / M_0 b)^{1/2} = 0.73$  nm. The refined criterion for loose grafting in the experiments is  $z < (b/a)N^{1/2} =$ 11. As a result, the NPs with z = 32 and 19 are densely grafted, while the NPs with z = 10 are in the crossover from loosely to

Macromolecules

densely grafted regimes. Next we estimate the structure of the grafted NPs in the experiments. Suppose a strand in the dry layer surrounding the particle contains x Kuhn monomers; then xsatisfies  $(4\pi/3)(d/2)^3 + zx(ba^2) = (4\pi/3)(d/2 + x^{1/2}b)^3$ . Note that the contribution of the particle volume to the dry core volume is considered. For the NPs with  $(z_1N_{tail}) = (32,30)$ , (19,39), and (10,39), we obtain x = 0, meaning that the dry core consists only of the particle. The overall size of a grafted NP is approximated by the size of a swollen star  $R_{\rm star} \approx b N_a^{3/5} (z/N)^{1/5}$ with  $N_a \approx N_{\text{tail}}$ . For  $(z, N_{\text{tail}}) = (32, 30)$ , (19, 39), and (10, 39), the estimated overall size ≈12.3, 12.9, and 11.4 nm. Experiments found that the hydrodynamic radii of the NPs in the three samples  $R_{\rm H} \approx 10^{\circ}$  nm. <sup>29</sup> This result roughly agrees with the estimated overall size of the densely grafted NPs, supporting the scaling description that the hydrodynamic radius  $R_H$  of a densely grafted NP with  $R_{\text{tail}} > d$  is dominated by  $R_{\text{tail}}$ . Note that hydrodynamic interactions in a semidilute polymer solution are screened on a length scale comparable to that for the screening of the intermolecular interactions. The melt chains drain through the grafted polymer brush on the length scale of the last correlation blob size  $\zeta_{\text{last}}$  (see Figure 5). As a result,  $R_{\text{H}} \approx$  $R_{\text{tail}} - C_{\zeta} \zeta_{\text{last}}$ , where  $C_{\zeta}$  is a numerical coefficient of order unity.<sup>31</sup>

Below we discuss the extension of the experiments to singletail NPs and loosely grafted multitail NPs. Consider an Fe<sub>3</sub>O<sub>4</sub> NP with d = 4.3 nm in a melt of PMMA chains with N = 26 Kuhn monomers per chain and chain size  $R \approx bN^{1/2} = 7.8$  nm. A single grafted PMMA chain would control the motion of the Fe<sub>3</sub>O<sub>4</sub> particle if the grafted chain size  $R_{\text{tail}} > b(d/b)^{3/2} \approx 7.2$  nm or the number of Kuhn monomers in the chain  $N_{\text{tail}} > 22$ , according to eq 8 for a single-tail NP with b < d < R. At  $N_{\text{tail}} = 22$ , the friction coefficients  $\zeta_{tail}$  and  $\zeta_{bare}$  of the PMMA tail and the bare Fe<sub>3</sub>O<sub>4</sub> particle are almost the same. Therefore, the diffusion coefficient of a single-tail NP with  $N_{\text{tail}} = 22$  is approximately half of that of a bare NP without the tail. For multiple grafted PMMA chains, the condition for loose grafting is  $z < (b/a)N^{1/2} = 11$ . If z = 6 PMMA chains were loosely grafted to a NP, no PMMA chains are in the dry core (as in the more densely grafted cases with z = 10, 19, and 32). The PPMA chains with less than  $(N/z)^2 = 19$  Kuhn monomers per chain form a Gaussian brush. There is no hydrodynamic coupling between the tails in the Gaussian brush, and the overall friction coefficient of the tails is  $6\zeta_{\text{tail}}$ . For d = 4.3nm < R=7.8 nm, the z=6 chains would control the motion of the Fe<sub>3</sub>O<sub>4</sub> particle if  $R_{\rm tail}>b(d/b)^{3/2}/z^{1/2}\approx 2.9$  nm or  $N_{\rm tail}>4$ , according to eq 14 for a NP grafted with a Gaussian brush. At  $N_{\text{tail}}$  = 4, the friction coefficient of the Gaussian brush  $6\zeta_{\text{tail}}$  is comparable to that of the bare particle  $\zeta_{\rm bare}$  and therefore reduces the diffusion coefficient of the particle by 50% with respect to that of the bare particle.

#### 4. CONCLUSIONS

We study the motion of a polymer-tethered NP in a polymer melt using scaling analysis. For a single-tail NP in an unentangled polymer melt, the friction coefficient  $\zeta(t)$  for the single-tail NP includes the contributions  $\zeta_{\rm bare}(t)$  from the bare NP and  $\zeta_{\rm tail}(t)$  from the tail. The competition between  $\zeta_{\rm bare}(t)$  and  $\zeta_{\rm tail}(t)$  determines whether the single-tail NP motion is dominated by the bare NP or the tail. In the particle-dominated regime,  $\zeta(t) \approx \zeta_{\rm bare}(t) > \zeta_{\rm tail}(t)$ , and the mean squared displacements of the tailed NP  $\langle \Delta r^2(t) \rangle$  is approximated as  $\langle \Delta r^2(t) \rangle_{\rm bare}$  for the bare NP. In a tail-dominated regime,  $\langle \Delta r^2(t) \rangle_{\rm bare}$  for the bare NP. In a tail-dominated regime,  $\langle \Delta r^2(t) \rangle_{\rm bare}$  for the smaller than a crossover time  $\tau^*$ , but  $\langle \Delta r^2(t) \rangle_{\rm tail}$  for  $t > \tau^*$ , as  $\zeta(t) \approx \zeta_{\rm tail}(t) > \zeta_{\rm bare}(t)$  for  $t > \tau^*$ . We

construct a diagram of regimes (Figure 1b) to show the particle-dominated regime and various tail-dominated regimes in the parameter space (d,R<sub>tail</sub>). The tail-dominated regimes differ in the tail dynamics that controls the single-tail NP motion (see Figure 3) and the crossover time  $\tau^*$  at which the tail-dominated motion begins (see Table 1).

The model of a multitail NP in an unentangled polymer melt can be mapped onto a corresponding star polymer in the same melt. A Gaussian brush region where chain segments adopt ideal random-walk conformations exists for loosely grafted tails with 1  $< z < N^{1/2}$ , but it is absent for densely grafted tails with  $z > N^{1/2}$ . For loosely grafted short tails with  $d < R_{tail} < bz$ , a multitail NP corresponds to a dry star diffusing in the melt with hydrodynamic radius  $\approx R_{\text{tail}}$ . With intermediate grafted chain size bz <  $R_{\text{tail}} < bN/z$ , a loosely grafted multitail NP corresponds to a star with a dry core (Figure 5c) and a Gaussian brush corona (Figure 5d). Similar to the motion of a single-tail NP, the motion of such a multitail NP can be in the particle-dominated regime or one of many tail-dominated regimes in the parameter space  $(d_iR_{tail})$ (see Figure 6). If the tails are sufficiently long with  $R_{tail} > bN/z$ , a loosely grafted multitail NP corresponds to a star with either a swollen brush corona (Figure 5e) or a swollen brush surrounded by Daoud-Cotton brush corona (Figure 5f). For the diffusion of such a multitail NP, the particle and the tails are hydrodynamically coupled. The tails with  $R_{\text{tail}} > d$  control the diffusion of the multitail NP, as  $R_{tail}$  dominates the hydrodynamic radius approximated by  $R_{\text{tail}} + d$ . The crossover time  $\tau^*$ for a tail-dominated regime of multitail NP motion is reduced with respect to the counterpart for single-tail NP motion (see Table 2 and Figure 2). For densely grafted tails with  $z > N^{1/2}$ , depending on the grafted chain size, a multitail NP corresponds to either a dry star or a star consisting of a dry core and a brush corona with no Gaussian region. In both scenarios, the densely grafted multitail NP diffuses in the melt with the hydrodynamic radius  $\approx R_{tail} + d$ , which is dominated by  $R_{tail}$  for  $R_{tail} > d$ .

In conclusion, our scaling theory for the mobility of polymertethered NPs in polymer melts demonstrates the interplay between the dynamics of the bare NP and the dynamics of the tethered polymer tails. The theory can be extended to polymertethered NPs in entangled polymer melts. As in unentangled polymer melts, the mobility of tethered particles in entangled polymer melts is dominated by the lower of the two mobilities: of the bare particle or of the tails. Bare particles with sizes smaller than the entanglement mesh size a behave essentially the same as those in unentangled polymer melts. However, the mobility of particles is significantly reduced as the particle size exceeds the tube diameter a of the melt. While sufficiently large particles are confined by the entanglement network with the mobility determined by the melt viscosity, particles only moderately larger than a can diffuse through the hopping mechanism and exhibit mobility higher than the prediction of the Stokes-Einstein relation. <sup>19</sup> For a single-tail NP, the particle participates in the reptation dynamics of the long tail if the tail has a lower mobility. For a multitail NP, the mobility of the tails can be approximated as that of a star polymer undergoing arm retraction in the same melt. The lower of the mobility of the bare particle and the corresponding star polymer determines the mobility of the multitail NP. Detailed theoretical description of the mobility of tethered NPs in entangled polymer melts will be presented in a future publication. One can also extend the present theory to study the mobility of a NP with an adsorption layer in a polymer melt by describing the adsorption layer as loops and tails. 15-17 Furthermore, the theory can be generalized

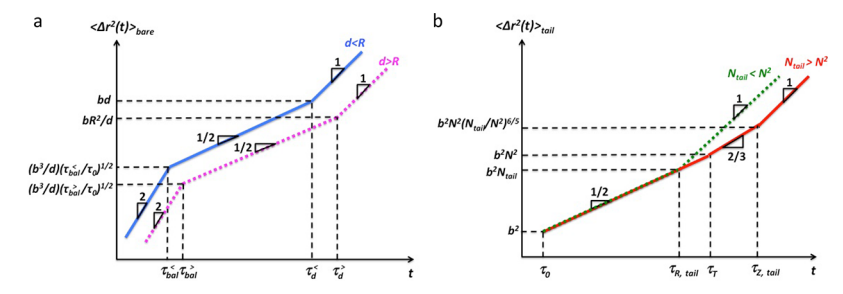


Figure A.1. (a) MSD  $\langle \Delta r^2(t) \rangle_{\text{bare}}$  of a bare NP with d < R (blue solid line) and d > R (magenta dotted line) in a melt of unentangled polymers with chain size R. (b) MSD  $\langle \Delta r^2(t) \rangle_{\text{tail}}$  for monomers in an unattached (free) tail polymer with  $N_{\text{tail}} < N^2$  (green dotted line) and  $N_{\text{tail}} > N^2$  (red solid line) in a melt of unentangled polymers with N monomers per chain.

to investigate the motion of a NP with reversibly grafted or adsorbed polymer chains.

# APPENDIX

# A. MSD of a Single-Tail NP in an Unentangled Polymer Melt

The MSD  $\langle \Delta r^2(t) \rangle_{\rm bare}$  of a bare nonsticky NP in an unentangled polymer melt has been calculated using scaling theory. The results of  $\langle \Delta r^2(t) \rangle_{\rm bare}$  are shown in Figure A.1a. The first scaling regime

$$\langle \Delta r^2(t) \rangle_{\rm bare} \approx \frac{k_{\rm B}T}{m} t^2 \quad {
m for} \quad t < au_{\rm bal}$$
 (A.1)

corresponds to the ballistic motion of the bare NP at time scales shorter than the ballistic time  $\tau_{\rm bal}$ . Subsequent scaling regimes describe the thermal motion of the NP. The subdiffusive regime with

$$\langle \Delta r^2(t) \rangle_{\text{bare}} \approx \left( \frac{b^3}{d} \right) \left( \frac{t}{\tau_0} \right)^{1/2} \quad \text{for} \quad \tau_{\text{bal}} < t < \tau_{\text{d}}$$
(A.2)

results from the coupling between the NP motion and the Rouse dynamics of the unentangled polymers up to the diffusion time  $\tau_{\rm d}$ . Matching eq A.1 and eq A.2, one obtains the ballistic time as the crossover time between the ballistic and subdiffusive regime

$$\tau_{\rm bal} \approx \tau_0 \left(\frac{mb}{\zeta_0 \tau_0 d}\right)^{2/3}$$
(A.3)

where  $\zeta_0$  is the monomeric friction coefficient and

$$\tau_0 \approx \frac{\zeta_0 b^2}{k_{\rm B} T} \tag{A.4}$$

is the monomer relaxation time. The subdiffusion of a NP with b < d < R is coupled to the relaxation of chain segments with sizes up to d, while the subdiffusion of a NP with d > R is coupled to the relaxation of the entire polymer chain. As a result, the diffusion time for the onset of Brownian motion of a NP is

$$\tau_{\rm d} \approx \begin{cases} \tau_0 \left(\frac{d}{b}\right)^4 \approx \tau_{\rm R} \left(\frac{d}{R}\right)^4 & \text{for } b < d < R \\ \tau_{\rm R} & \text{for } b < d < R \end{cases}$$
(A.5)

where  $\tau_{\rm R} \approx \tau_0 N^2 \approx \tau_0 (R/b)^4$  is the Rouse relaxation time of the polymer melt. The final scaling regime with  $t > \tau_{\rm d}$  corresponds to NP diffusion with MSD increasing linearly with time

$$\langle \Delta r^{2}(t) \rangle_{\text{bare}} \approx \begin{cases} \frac{b^{3}}{Nd} \left(\frac{R}{d}\right)^{2} \left(\frac{t}{\tau_{0}}\right) & \text{for } b < d < R \\ \frac{b^{3}}{Nd} \left(\frac{t}{\tau_{0}}\right) & \text{for } d > R \end{cases}$$
(A.6)

The MSD  $\langle \Delta r^2(t) \rangle_{\rm tail}$  of monomers in a linear polymer containing  $N_{\rm tail}$  monomers is obtained based on scaling models for the dynamics of unentangled polymers. Scaling descriptions of  $\langle \Delta r^2(t) \rangle_{\rm tail}$  are presented in Figure A.1b. A shorter polymer with  $N_{\rm tail} < N^2$  relaxes by Rouse dynamics, and

where  $au_{\rm R,tail} \approx au_0 {N_{\rm tail}}^2$  is the Rouse time. The shorter polymer finally diffuses with

$$\langle \Delta r^2(t) \rangle_{\rm tail} \approx R_{\rm tail}^2 \left( \frac{t}{\tau_{\rm R,tail}} \right) \approx b^2 N_{\rm tail} \left( \frac{t}{\tau_{\rm R,tail}} \right) \quad {
m for}$$

$$N_{\rm tail} < N^2 \text{ and } t > \tau_{\rm R,tail}$$
(A.8)

A longer polymer with  $N_{\rm tail} > N^2$  first relaxes by Rouse dynamics until  $\tau_{\rm T} \approx \tau_0 N^4$ , which is the relaxation time of a chain segment containing  $N^2$  monomers, and then it relaxes by Zimm dynamics until the Zimm time  $\tau_{\rm Z,tail} \approx \tau_{\rm T} (N_{\rm tail}/N^2)^{9/5}$ . Zimm dynamics occurs at time scales  $t > \tau_{\rm T}$ , as the hydrodynamic coupling between sections of the long polymer can no longer be screened by the shorter melt chains. For the Rouse dynamics and the subsequent Zimm dynamics, the MSD of monomers is

$$\begin{split} \langle \Delta r^2(t) \rangle_{\rm tail} &\approx \begin{cases} b^2 \bigg( \frac{t}{\tau_0} \bigg)^{1/2} & \text{for } N_{\rm tail} > N^2 \text{ and } \\ & \tau_0 < t < \tau_{\rm T} \end{cases} \\ b^2 N^2 \bigg( \frac{t}{\tau_{\rm T}} \bigg)^{2/3} & \text{for } N_{\rm tail} > N^2 \text{ and } \\ & \tau_{\rm T} < t < \tau_{\rm Z, tail} \end{cases} \end{split} \tag{A.9}$$

Finally, the long polymer diffuses with

$$\langle \Delta r^2(t) \rangle_{\text{tail}} \approx R_{\text{tail}}^2 \left( \frac{t}{\tau_{\text{Z,tail}}} \right) \approx b^2 N^2 \left( \frac{N_{\text{tail}}}{N^2} \right)^{6/5} \left( \frac{t}{\tau_{\text{Z,tail}}} \right) \quad \text{for}$$
 $N_{\text{tail}} > N^2 \quad \text{and} \quad t > \tau_{\text{Z,tail}}$  (A.10)

For  $d < R_{\text{tail}} < bN$ , the MSD  $\langle \Delta r^2(t) \rangle$  of a single-tail NP is obtained based on the approximation in eq 10. Below we describe the time dependence of  $\langle \Delta r^2(t) \rangle$  for different tail-dominated scaling regimes in the  $(d_rR_{\text{tail}})$  parameter space (see Figure 1b).

Regime I: Small NP with b < d < R and Long tail with  $b(d/b)^{3/2} < R_{tail} < bN$  (SL). The time dependence of  $\langle \Delta r^2(t) \rangle$  in regime I is shown by the blue dashed line in Figure 3a.  $\langle \Delta r^2(t) \rangle \approx \langle \Delta r^2(t) \rangle_{\text{bare}} \sim t^2$  (eq A.1) for  $t < \tau_{\text{bab}} \sim t^{1/2}$  (eq A.2) for  $\tau_{\text{bal}} < t < \tau_d^I$ , and  $\sim t$  (eq A.6) for  $\tau_d^I < t < \tau_l^T$ . Subsequently,  $\langle \Delta r^2(t) \rangle \approx \langle \Delta r^2(t) \rangle_{\text{tail}} \sim t^{1/2}$  (eq A.7) for  $\tau_l^* < t < \tau_{\text{R,fail}}$  and  $\sim t$  (eq A.8) for  $t > \tau_{\text{R,fail}}$ .

Regime II: Small NP with b < d < R and Very long tail with  $R_{\text{tail}} > bN$  (SV). The time dependence of  $\langle \Delta r^2(t) \rangle$  in regime II is shown by the magenta dashed line in Figure 3b. The crossover time  $\tau_{II}^* \approx \tau_I^*$  (see Table 1) and the time dependence of  $\langle \Delta r^2(t) \rangle$  for  $t < \tau_{II}^*$  in regime II is identical to that for  $t < \tau_I^*$  in regime I. Above the crossover time,  $\langle \Delta r^2(t) \rangle \approx \langle \Delta r^2(t) \rangle_{\text{tail}} \sim t^{1/2}$  and  $\sim t^{2/3}$  (eq A.9) for  $\tau_{II}^* < t < \tau_T$  and  $\tau_T < t < \tau_{Z,\text{tail}}$ , respectively. Finally,  $\langle \Delta r^2(t) \rangle \approx \langle \Delta r^2(t) \rangle_{\text{tail}} \sim t$  (eq A.10) for  $t > \tau_{Z,\text{tail}}$ . Compared with regime I, regime II has an additional time dependence  $\langle \Delta r^2(t) \rangle \sim t^{2/3}$ , which is due to the Zimm dynamics of a very long tail with  $R_{\text{tail}} > bN$ .

Regime III: Large NP with R < d < bN and Long tail with  $R(d/b)^{1/2} < R_{\rm tail} < bN$  (LL). The time dependence of  $\langle \Delta r^2(t) \rangle$  in regime III (red solid line in Figure 3a) is similar to that in regime I (blue dashed line in Figure 3a). One difference between regime III and regime I is that  $\tau_{\rm d}^{\rm III} \approx \tau_{\rm R}$ , while  $\tau_{\rm d}^{\rm I} \approx \tau_{\rm R}(d/R)^4 < \tau_{\rm R}$  (see eq A.5). Another difference is in the d-dependence of the crossover time,  $\tau_{\rm III}^* \approx \tau_0 (d/b)^2 (R/b)^4$ , whereas  $\tau_{\rm I}^* \approx \tau_0 (d/b)^6$  (see Table 1).

Regime IV: Large NP with R < d < bN and Very long tail with  $R_{\rm tail} > bN$  (LV). Regime IV and regime II have a similar time dependence of  $\langle \Delta r^2(t) \rangle$  (see green dotted line and magenta dashed line in Figure 3b). The differences between regime IV and regime II are identical to those between regime III and regime II:  $(1) \ \tau_{\rm d}^{\rm IV} \approx \tau_{\rm d}^{\rm II} \approx \tau_{\rm R} \ {\rm versus} \ \tau_{\rm d}^{\rm II} \approx \tau_{\rm R} (d/R)^4 \ {\rm and} \ (2) \ \tau_{\rm IV}^{\rm IV} \approx \tau_{\rm III}^{\rm II} \approx \tau_0 (d/b)^2 (R/b)^4 \ {\rm versus} \ \tau_{\rm II}^{\rm II} \approx \tau_{\rm I}^* \approx \tau_0 (d/b)^6.$ 

Regime V: Very large NP with d > bN and Very long tail with  $R_{\text{tail}} > d$  (VV). As shown by the cyan solid line in Figure 3b,  $\langle \Delta r^2(t) \rangle \approx \langle \Delta r^2(t) \rangle_{\text{bare}} \sim t^2$  (eq A.1) for  $t < \tau_{\text{bab}}, \sim t^{1/2}$  (eq A.2) for  $\tau_{\text{bal}} < t < \tau_{\text{d}}^V$ , and  $\sim t$  (eq A.6) for  $\tau_{\text{d}}^V < t < \tau_{\text{t}}^*$ . Above the crossover time  $\tau_{\text{t}}^*$ ,  $\langle \Delta r^2(t) \rangle \approx \langle \Delta r^2(t) \rangle_{\text{tail}} \sim t^{2/3}$  (eq A.9) for  $\tau_{\text{t}}^* < t < \tau_{\text{z,tail}}$  and finally  $\sim t$  (eq A.10) for  $t > \tau_{\text{z,tail}}$ . Since the crossover time  $\tau_{\text{t}}^* > \tau_{\text{T}}$ , the tailed NP does not participate in the Rouse dynamics of the tail. As a result, there is no time range with  $\langle \Delta r^2(t) \rangle \sim t^{1/2}$  for  $t > \tau_{\text{t}}^*$  in regime V.

## B. Motion of a NP Tethered with a Dry Layer in an Unentangled Polymer Melt

Consider a NP with  $1 < z < N^{1/2}$  loosely grafted tails and  $d < R_{\rm tail}$  < bz. The grafted layer is dry, as  $R_{\rm tail}$  is smaller than the dry core size bz of the corresponding star polymer (see Figure 5a). Below we show that the mean square fluctuation of the NP under the confinement of the grafted layer is smaller than the MSD of a dry sphere with size  $\approx R_{\rm tail}$  in the matrix of melt chains. As a result, the motion of the tethered NP is approximated as that of the dry sphere with size  $\approx R_{\rm tail}$ .

Suppose a coherently moving segment of a tail in the dry layer contains g(t) monomers at time t. The fluctuation of the size of a segment containing g monomers is  $r_g \approx b g^{1/2}$ . The relaxation time of the segment is approximately the time it takes for the segment with diffusion coefficient  $\approx k_{\rm B}T/(\zeta_0 g)$  to diffuse a distance comparable to the fluctuation of its size; that is,  $\tau_g \approx r_g^2/$ 

 $(k_{\rm B}T/\zeta_0g) \approx au_0g^2$ . As a result,  $g(t) \approx (t/ au_0)^{1/2}$ . The mean square fluctuation of the particle confined by the tethered chains is  $\langle \Delta r^2(t) \rangle_{\rm f} \approx b^2 g(t)/z \approx b^2 (t/ au_0)^{1/2}/z$ . Note that  $\langle \Delta r^2(t) \rangle_{\rm f}$  is smaller than the MSD  $\langle \Delta r^2(t) \rangle_{\rm bare}$  of a bare NP in the same dry layer. The viscosity of a melt consisting of chains with g monomers per chain is  $\eta_g \approx (k_{\rm B}T/b^3g)\tau_g \approx \eta_0 g$ . The effective viscosity experienced by the bare particle at time scale t is  $\eta_g(t) \approx \eta_0 g(t) \approx \eta_0 (t/ au_0)^{1/2}$ , and the effective friction coefficient  $\zeta(t) \approx \eta_g(t) d \approx \zeta_0 (d/b) (t/ au_0)^{1/2}$ . As a result,  $\langle \Delta r^2(t) \rangle_{\rm bare} \approx [k_{\rm B}T/\zeta(t)]t \approx (b^3/d)(t/ au_0)^{1/2}$ . For d < bz,  $\langle \Delta r^2(t) \rangle_{\rm bare} > b^2(t/ au_0)^{1/2}/z \approx \langle \Delta r^2(t) \rangle_{\rm b}$  which means the confinement of tethered chains reduces the mobility of the particle with respect to the bare particle in the same dry layer.

The MSD of a dry sphere with diameter  $\approx R_{tail} < bz$  in the matrix of melt chains with chain size  $R \approx bN^{1/2} > bz$  is  $\langle \Delta r^2(t) \rangle_{dry} \approx (b^3/R_{tail})(t/\tau_0)^{1/2}$  (see eq A.2) for  $t < \tau_0(R_{tail}/b)^4$  (see eq A.5). The ratio  $\langle \Delta r^2(t) \rangle_{dry}/\langle \Delta r^2(t) \rangle_f \approx bz/R_{tail} > 1$  for  $R_{tail} < bz$ . Therefore, the MSD of the dry sphere dominates over the mean square fluctuation of the particle confined by the tethered chains. Accordingly, we approximate the MSD of the NP with a loosely grafted dry layer as

$$\langle \Delta r^2(t) \rangle \approx \langle \Delta r^2(t) \rangle_{\rm dry} \approx \frac{b^3}{R_{\rm tail}} \left( \frac{t}{\tau_0} \right)^{1/2} \quad {
m for}$$

$$1 < z < N^{1/2} \quad {\rm and} \quad t < \tau_0 \left( \frac{R_{\rm tail}}{b} \right)^4 \tag{B.1}$$

while  $\langle \Delta r^2(t) \rangle_{\rm f} < \langle \Delta r^2(t) \rangle$  is the internal fluctuation of the particle position.

Next, consider a NP with  $z > N^{1/2}$  densely grafted tails and  $d < R_{\rm tail} < bz^{1/2}N^{1/4}$ , where  $bz^{1/2}N^{1/4}$  is the dry core size of the corresponding star polymer (see Figure 5b). Similar to the result for a loosely tethered NP, the mean square fluctuation  $\langle \Delta r^2(t) \rangle_{\rm fr} \approx b^2(t/\tau_0)^{1/2}/z$ , and it is smaller than  $\langle \Delta r^2(t) \rangle_{\rm bare}$  of the bare particle in the same dry chains. The MSD of a dry sphere with diameter  $\approx R_{\rm tail}$  in the melt chains with chain size R is  $\langle \Delta r^2(t) \rangle_{\rm dry} \approx (b^3/R_{\rm tail})(t/\tau_0)^{1/2}$  (see eq A.2) at times smaller than the diffusion time  $\tau_{\rm d}$ . According to eq A.5,  $\tau_{\rm d} \approx \tau_0 (R_{\rm tail}/b)^4$  if  $R_{\rm tail} < R$ , whereas  $\tau_{\rm d} \approx \tau_{\rm R} \approx \tau_0 (R/b)^4$  if  $R < R_{\rm tail} < bz^{1/2}N^{1/4}$ . The ratio  $\langle \Delta r^2(t) \rangle_{\rm dry}/\langle \Delta r^2(t) \rangle_{\rm f} \approx (bz/R_{\rm tail}) > z^{1/2}/N^{1/4} > 1$  for  $R_{\rm tail} < bz^{1/2}N^{1/4}$  and  $z > N^{1/2}$ . As a result, the MSD of the NP with a densely grafted dry layer is

$$\langle \Delta r^{2}(t) \rangle \approx \langle \Delta r^{2}(t) \rangle_{\text{dry}} \approx \frac{b^{3}}{R_{\text{tail}}} \left( \frac{t}{\tau_{0}} \right)^{1/2} \quad \text{for} \quad z > N^{1/2}$$
and  $t < \tau_{\text{d}} \approx \tau_{0} \left( \frac{\min\{R_{\text{tail}}, R\}}{b} \right)^{4}$ 
(B.2)

with the internal fluctuation of the particle position  $\langle \Delta r^2(t) \rangle_{\rm f} < \langle \Delta r^2(t) \rangle$ .

# AUTHOR INFORMATION

## **Corresponding Author**

\*E-mail: michael.rubinstein@duke.edu.

ORCID ®

Ting Ge: 0000-0003-2456-732X

#### Notes

The authors declare no competing financial interest.

#### ACKNOWLEDGMENTS

We acknowledge financial support from National Science Foundation under Grant Nos. DMR-1121107 and EFMA-1830957, the National Institutes of Health under Grant Nos. P01-HL108808, R01-HL136961, and 5UH3HL123645, and the Cystic Fibrosis Foundation.

### REFERENCES

- (1) Ye, X.; Tong, P.; Fetters, L. J. Transport of Probe Particles in Semidilute Polymer Solutions. *Macromolecules* **1998**, *31*, 5785–5793.
- (2) Omari, R. A.; Aneese, A. M.; Grabowski, C. A.; Mukhopadhyay, A. Diffusion of Nanoparticles in Semidilute and Entangled Polymer Solutions. *J. Phys. Chem. B* **2009**, *113*, 8449–8452.
- (3) Tuteja, A.; Mackay, M. E.; Hawker, C. J.; Van Horn, B. Effect of Ideal, Organic Nanoparticles on the Flow Properties of Linear Polymers: Non-Einstein-like Behavior. *Macromolecules* **2005**, *38*, 8000–8011.
- (4) Guo, H.; Bourret, G.; Corbierre, M. K.; Rucareanu, S.; Lennox, R. B.; Laaziri, K.; Piche, L.; Sutton, M.; Harden, J. L.; Leheny, R. L. Nanoparticle Motion within Glassy Polymer Melts. *Phys. Rev. Lett.* **2009**, *102*, 075702.
- (5) Guo, H.; Bourret, G.; Lennox, R. B.; Sutton, M.; Harden, J. L.; Leheny, R. L. Entanglement-Controlled Subdiffusion of Nanoparticles within Concentrated Polymer Solutions. *Phys. Rev. Lett.* **2012**, *109*, 055901.
- (6) Grabowski, C. A.; Mukhopadhyay, A. Size Effect of Nanoparticle Diffusion in a Polymer Melt. *Macromolecules* **2014**, *47*, 7238–7242.
- (7) Balazs, A. C.; Emrick, T.; Russell, T. P. Nanoparticle polymer composites: Where two small worlds meet. *Science* **2006**, *314*, 1107–1110.
- (8) Karatrantos, A.; Composto, R. J.; Winey, K. I.; Clarke, N. Polymer and spherical nanoparticle diffusion in nanocomposites. *J. Chem. Phys.* **2017**, *146*, 203331.
- (9) Schuster, B. S.; Ensign, L. M.; Allan, D. B.; Suk, J. S.; Hanes, J. Particle tracking in drug and gene delivery research: state-of-the-art applications and methods. *Adv. Drug Delivery Rev.* **2015**, *91*, 70–91.
- (10) Voylov, D. N.; Holt, A. P.; Doughty, B.; Bocharova, V.; Meyer, H. M.; Cheng, S.; Martin, H.; Dadmun, M.; Kisliuk, A.; Sokolov, A. P. Unraveling the Molecular Weight Dependence of Interfacial Interactions in Poly(2-vinylpridine)/Silica Nanocomposites. *ACS Macro Lett.* 2017, 6, 68–72.
- (11) Cheng, S.; Carroll, B.; Bocharova, V.; Carrillo, J.-M. Y.; Sumpter, B. G.; Sokolov, A. P. Focus: Structure and dynamics of the interfacial layer in polymer nanocomposites with attractive interactions. *J. Chem. Phys.* **2017**, *146*, 203201.
- (12) Lai, S. K.; Wang, Y.-Y.; Wirtz, D.; Hanes, J. Micro- and macrorheology of mucus. *Adv. Drug Delivery Rev.* **2009**, *61*, 86–100.
- (13) Eisenriegler, E. Polymer Near Surfaces: Conformation Properties and Relation to Critical Phenomena; World Scientific Publishing Co. Pte. Ltd., 1993.
- (14) Guiselin, O. Irreversible Adsorption of a Concentrated Polymer Solution. *Europhys. Lett.* **1992**, *17*, 225–230.
- (15) Scheutjens, J. M. H. M.; Fleer, G. J. Statistical theory of the adsorption of interacting chain molecules. 2. Train, loop, and tail size distribution. *J. Phys. Chem.* **1980**, *84*, 178–190.
- (16) Semenov, A. N.; Joanny, J.-F. Structure and Adsorbed Polymer Layers: Loops and Tails. *Europhys. Lett.* **1995**, *29*, 279.
- (17) Ge, T.; Rubinstein, M. Strong Selective Adsorption of Polymers. *Macromolecules* **2015**, *48*, 3788–3801.
- (18) Cai, L. H.; Panyukov, S.; Rubinstein, M. Mobility of Nonsticky Nanoparticles in Polymer Liquids. *Macromolecules* **2011**, *44*, 7853–7863.
- (19) Cai, L. H.; Panyukov, S.; Rubinstein, M. Hopping Diffusion of Nanoparticles in Polymer Matrices. *Macromolecules* **2015**, *48*, 847–862
- (20) Rubinstein, M.; Colby, R. H. *Polymer Physics*; Oxford University Press, 2003.

(21) Daoud, M.; Cotton, J. P. Star shaped polymers: a model for the conformation and its concentration dependence. *J. Phys.* (*Paris*) **1982**, 43, 531–538.

- (22) Raphael, E.; Pincus, P.; Fredrickson, G. H. Conformation of Star Polymers in High Molecular Weight Solvents. *Macromolecules* **1993**, *26*, 1996–2006.
- (23) Aubouy, M.; Fredrickson, G. H.; Pincus, P.; Raphaeel, E. End-Tethered Chains in Polymeric Matrices. *Macromolecules* **1995**, 28, 2979–2981.
- (24) Gay, C.; Raphaël, E. Static Properties of a Star Polymer in a High Molecular Weight Solvent. *J. Phys. II* **1996**, *6*, 587–591.
- (25) Kandar, A. K.; Srivastava, S.; Basu, J. K.; Mukhopadhyay, M. K.; Seifert, S.; Narayanan, S. Unusual dynamical arrest in polymer grafted nanoparticles. *J. Chem. Phys.* **2009**, *130*, 121102.
- (26) Hoshino, T.; Murakami, D.; Tanaka, Y.; Takata, M.; Jinnai, H.; Takahara, A. Dynamical crossover between hyperdiffusion and subdiffusion of polymer-grafted nanoparticles in a polymer matrix. *Phys. Rev. E* **2013**, *88*, 032602.
- (27) Liu, S.; Senses, E.; Jiao, Y.; Narayanan, S.; Akcora, P. Structure and Entanglement Factors on Dynamics of Polymer-Grafted Nanoparticles. *ACS Macro Lett.* **2016**, *5*, 569–573.
- (28) Choi, J.; Hore, M. J. A.; Clarke, N.; Winey, K. I.; Composto, R. J. Nanoparticle Brush Architecture Controls Polymer Diffusion in Nanocomposites. *Macromolecules* **2014**, *47*, 2404–2410.
- (29) Lin, C.-C.; Griffin, P. J.; Chao, H.; Hore, M. J. A.; Ohno, K.; Clarke, N.; Riggleman, R. A.; Winey, K. I.; Composto, R. J. Grafted polymer chains suppress nanoparticle diffusion in athermal polymer melts. *J. Chem. Phys.* **2017**, *146*, 203332.
- (30) Lin et al.<sup>29'</sup> used b = 1.96 nm for the Kuhn monomer size of PMMA. The value b = 1.53 nm we use in this paper is from Table 25.3 in Chapter 25 of *Physical Properties of Polymers Handbook*, 2nd ed.; edited by J. E. Mark, Springer Science + Business Media, LLC: New York, 2007.
- (31) Zhulina, E. B.; Adam, M.; LaRue, I.; Sheiko, S. S.; Rubinstein, M. Diblock Copolymer Micelles in a Dilute Solution. *Macromolecules* **2005**, 38, 5330–5351.